JOURNAL OF GEOPHYSICAL RESEARCH, VOL. 112, D09316, doi:10.1029/2006JD007792, 2007

A set of diagnostics for evaluating chemistry-climate models in the extratropical tropopause region

L. L. Pan,[1] J. C. Wei,[2,3] D. E. Kinnison,[1] R. R. Garcia,[1] D. J. Wuebbles,[2] and G. P. Brasseur[1]

Received 14 July 2006; revised 6 December 2006; accepted 13 December 2006; published 15 May 2007.

[1] Three related diagnostics are used to evaluate the representation of chemical transport processes in the extratropical upper troposphere and lower stratosphere (UTLS) by chemistry-transport and chemistry-climate models. The diagnostics are based on in situ observations of ozone, carbon monoxide, water vapor profiles (obtained on board the NASA ER-2 research aircraft, near 65°N and during 1997), and their interrelationships in the UTLS. The first diagnostic compares the observed and modeled UTLS trace gas profiles in a relative altitude coordinate. The second one compares the observed and modeled UTLS tracer relationships. The third one compares the observed and modeled thickness of the tropopause transition layer. Together, they characterize the model's ability to reproduce the observed chemical distribution in the UTLS region and chemical transition across the extratropical tropopause. These are key indicators of whether the contributions of dynamics and chemistry to this region are correctly represented in the models. These diagnostics are used to evaluate the performance of an NCAR chemistry-transport model (CTM), MOZART-3, and a chemistry-climate model (CCM), WACCM3. Results from four model runs with different meteorological fields and grid resolution are examined. Overall, the NCAR models show qualitative agreement with the observations in the location of the chemical transition across the extratropical tropopause. Quantitatively, there are significant differences between the modeled and the observed chemical distributions. Both the meteorological field and grid resolutions are contributing factors to the differences.

Citation: Pan, L. L., J. C. Wei, D. E. Kinnison, R. R. Garcia, D. J. Wuebbles, and G. P. Brasseur (2007), A set of diagnostics for evaluating chemistry-climate models in the extratropical tropopause region, *J. Geophys. Res.*, *112*, D09316, doi:10.1029/2006JD007792.

1. Introduction

[2] Interactions between dynamics and chemistry in the region of the extratropical tropopause play a significant role in chemistry-climate coupling. Concentrations of several radiatively significant trace constituents, such as ozone and water vapor, change rapidly across the tropopause. Their gradients and variability in this region are controlled by their respective sources and sinks and the mixing and exchange between the stratosphere and troposphere. Accurate simulation of the distribution of radiatively significant chemical species is essential for the correct prediction of climate change by numerical models. With ongoing increases of horizontal and vertical resolution in global models, improved representation of gradients across the tropopause is expected. It is desirable to have a set of diagnostics to evaluate how well the tropopause region, and more generally the region of the upper troposphere and lower stratosphere (UTLS), is represented in the new generations of chemistry transport models (CTMs) and chemistry climate models (CCMs). The focus of this work is to describe a set of diagnostics for model evaluation in the tropopause region, as a part of the CCM community's ongoing effort of process-oriented validation [*Austin et al.*, 2003; *Eyring et al.*, 2005, and references therein].

[3] The rapid change of chemical composition across the tropopause is largely a consequence of the sharp changes in thermal and dynamical fields at this boundary. Physically, this boundary is created and maintained mainly by the balance of thermal relaxation and the stirring of baroclinic eddies [*Haynes et al.*, 2001]. The changes of the thermal and dynamical fields result in and maintain very different transport characteristics below and above the tropopause. The chemical discontinuity across the tropopause is therefore an important diagnostic of the model's transport scheme. In addition, the distribution of tracers provides an effective check of the chemistry calculated in the model, since the chemical tracers are also controlled by the chemical sources and sinks in the two regions.

[1] Atmospheric Chemistry Division, National Center for Atmospheric Research, Boulder, Colorado, USA.
[2] Department of Atmospheric Sciences, University of Illinois at Urbana-Champaign, Urbana, Illinois, USA.
[3] Now at QSS Group, Inc., Lanham, Maryland, USA.

0148-0227/07/2006JD007792$09.00

[4] We present a set of model diagnostics using observed changes in chemical tracer profiles and tracer-tracer correlations across the extratropical tropopause. The motivation is to examine (1) whether the models reproduce the observed chemical distribution in the UTLS region; (2) whether the models show a chemical discontinuity, i.e., abrupt change in chemical composition, across the extratropical tropopause similar to that observed; (3) whether the chemical transition simulated by models occurs near the thermal tropopause as observed; (4) whether the characteristics of the chemical transition vary with the meteorological fields used in the model; and (5) how the change of grid resolution impacts the modeled transition in terms of its location and sharpness.

[5] In situ measurements of ozone, water vapor and carbon monoxide near Fairbanks, Alaska (65°N) from the NASA ER-2 research aircraft during the 1997 Photochemistry of Ozone Loss in the Arctic Region in Summer (POLARIS) campaign [*Newman et al.*, 1999] are used in this analysis. Among the growing collection of aircraft measurements in the UTLS region, the POLARIS data set has several advantages. Chiefly, this data set provides vertical profile measurements from 5 to 18 km and covers well the range of altitude between the upper troposphere and lower stratosphere. The data set includes collocated temperature profiles, which allow an accurate identification of the tropopause altitude. The measurements took place at locations distant from the jet streams, and the chemical transition across the tropopause is well defined in these observations [*Pan et al.*, 2004]. Dynamically, the distribution of chemical species in the lowermost stratosphere in this latitudinal range is controlled by large-scale descent via the Brewer-Dobson circulation, and by isentropic transport and mixing from the subtropical UTLS [e.g., *Holton et al.*, 1995]. Examining the model results at this location will provide important information on the circulation and the transport scheme in the models.

[6] One of the main objectives of this paper is to demonstrate the value of tracer-tracer correlations as a diagnostic tool for models in the UTLS region. The tracer-correlation method is frequently used in UTLS data analyses, especially in analyses of aircraft data [e.g., *Fischer et al.*, 2000; *Marcy et al.*, 2004; *Ridley et al.*, 2004]. In particular, the correlations near the extratropical tropopause have been shown to be an effective method for diagnosing stratosphere-troposphere exchange and mixing across the tropopause [e.g., *Hintsa et al.*, 1998; *Zahn et al.*, 2000; *Hoor et al.*, 2002, 2004; *Zahn and Brenninkmeijer*, 2003; *Pan et al.*, 2004, 2006; *Hegglin et al.*, 2006]. The method has also been used in evaluating the performance of CTMs [e.g., *Hsu et al.*, 2004]. The theoretical framework for its general application in this region for transport diagnostics is not yet well established. Applications of tracer correlations in data remain empirical, and we emphasize the robust features that stand out from the wide range of variability. In this study, we examine the use of tracer correlations as model diagnostics in the extratropical UTLS region, following the method presented by *Pan et al.* [2004].

[7] The paper is divided into four sections. Following the introduction, the models and the data used are described in section 2. Section 3 presents the methods and the results of the diagnostics. Section 4 provides conclusions and discussions. The parameters derived from ER-2 data for model evaluation used in these three diagnostics are given in Appendix A.

2. Descriptions of Models and Observations

2.1. MOZART-3 Chemical-Transport Model

[8] The 3D chemical-transport Model for Ozone and Related chemical Tracers, version 3 (MOZART-3), was designed to represent the chemical and physical processes from the troposphere through the mesosphere. This model is an extension of the global tropospheric MOZART-1 and MOZART-2 CTMs [*Brasseur et al.*, 1998; *Hauglustaine et al.*, 1998; *Horowitz et al.*, 2003; *Emmons et al.*, 2003]. The chemical scheme accounts for processes specific to the troposphere through the mesosphere, and includes a representation of heterogeneous processes on sulfate aerosols and PSC particles. The MOZART-3 chemical mechanism includes 106 species and over 250 photochemical reactions. In all simulations, the chemical rate constants are taken from JPL02-25 [*Sanders et al.*, 2003]. Contained within the MOZART-3 framework, is the Model of Atmospheric Transport and Chemistry (MATCH) described by *Rasch et al.* [1997]. MATCH includes representations of deep and shallow convection, boundary layer mixing, and wet and dry deposition processes. Advection of chemical tracers is performed following *Lin and Rood* [1997]. A detailed description of MOZART-3 is given by D. E. Kinnison et al. (Sensitivity of chemical tracers to meteorological parameters in the MOZART-3 chemical transport model, submitted to *Journal of Geophysical Research,* 2006, hereinafter referred to as Kinnison et al., submitted manuscript, 2006). Several application studies using MOZART-3 have recently been published [*Forkman et al.*, 2003; *Park et al.*, 2004; *Sassi et al.*, 2004; *Gettelman et al.*, 2004; *Kulawik et al.*, 2006].

[9] In this study, MOZART-3 is driven with two meteorological analyses from the European Centre for Medium-Range Weather Forecasts (ECMWF). The first is the standard operational meteorological analysis, designated as Op in this study. The second is a new reanalysis product, designated as EXP471. Both the ECMWF Op and EXP471 analyses are based on a new 4D-Var approach developed at ECMWF. Discussion of these meteorological products is given by *Monge-Sanz et al.* [2007]. Significant improvement of EXP471 over the Op analysis is attributed to the use of an ω-equation balance operator in the background constraint. The resolution for both meteorological analyses is consistent with a T63 truncation to a Gaussian grid of horizontal resolution $1.9° \times 1.9°$, with 60 vertical levels from the surface to approximately 65 km. The vertical resolution is $\sim$0.8 km in the UTLS region, extending to 2 km in the middle and upper stratosphere. Both ECMWF Op and EXP471 meteorological fields are representative of the year 2000.

2.2. WACCM Coupled Chemistry Climate Model

[10] The Whole Atmosphere Community Climate Model, Version 3 (WACCM3) is a comprehensive numerical model, spanning the range of altitude from the Earth's surface to the thermosphere [*Sassi et al.*, 2004; *Garcia et al.*, 2007]. WACCM3 has 66 vertical levels from the ground

Table 1. Model Cases Used in the Analyses and Intercomparison[a]

Case	Framework	Meteorological Field	Chemistry (Number of Species)	Resolution (Horizontal, Vertical)
1	MOZART-3	ECMWF(Op)	106	1.9 × 1.9, ∼0.8 km
2	MOZART-3	ECMWF(EXP471)	106	1.9 × 1.9, ∼0.8 km
3	WACCM3	fully interactive	51	1.9 × 2.5, ∼1.1 km
4	WACCM3	fully interactive	51	4 × 5, ∼1.1 km

[a]The horizontal resolution is given in degrees of latitude × longitude, and the vertical resolution is given as the level separation near the tropopause. Note that in the runs with 51 chemical species (cases 3 and 4), the NMHCs are omitted in the chemistry.

to 5.1×10^{-6} hPa. The vertical resolution is variable: 3.5 km above 65 km, 1.75 km around the stratopause (50 km), 1.1–1.4 km in the lower stratosphere (below 30 km), and 1.1 km in the troposphere (except near the ground where the resolution is much higher in the planetary boundary layer). WACCM3 currently supports two horizontal resolutions: 1.9° × 2.5° and 4° × 5° (latitude × longitude) and results from both versions are shown in this study. WACCM3 is a superset of the Community Atmospheric Model, Version 3 (CAM3) and includes all of the physical parameterizations of CAM3 [*Collins et al.*, 2004]. WACCM3 is a fully interactive model, where the radiatively active gases (CO_2, H_2O, N_2O, CH_4, CFC-11, CFC-12, NO, O_2, O_3) affect heating and cooling rates and therefore dynamics and transport of trace constituents. The dynamical core of the model uses a conservative and shape preserving finite volume approach [*Lin*, 2004].

[11] WACCM3 includes a detailed neutral chemistry model for the middle atmosphere based on the MOZART-3, but without nonmethane hydrocarbon (NMHC) chemistry. The mechanism represents chemical and physical processes in the stratosphere through the lower thermosphere; tropospheric chemistry is fairly complete, except for the omission of NMHC chemistry, as noted above. The species included within this mechanism are contained within the O_X, NO_X, HO_X, ClO_X, and BrO_X chemical families, along with CH_4 and its degradation products. This mechanism contains 51 species, 118 gas phase reactions, 49 photolytic reactions, and 17 heterogeneous reactions on four aerosol types (LBS, STS, NAT, and water-ice). Details of the numerical solution approach, gas phase and heterogeneous processes are described by Kinnison et al. (submitted manuscript, 2006). In all simulations, the chemical rate constants are taken from JPL02-25 [*Sanders et al.*, 2003].

[12] For this study, both the 1.9° × 2.5° and 4° × 5° WACCM3 versions were run in a perpetually solar minimum environment. Both simulations were run for over 20 years. The lower boundary conditions (e.g., CH_4, CO_2, N_2O, and halogens; and SSTs) are consistent with the year 1995. The sulfate aerosol surface area density was also consistent with year 1995.

2.3. Ozone, Water Vapor, and Carbon Monoxide Data From POLARIS

[13] The POLARIS campaign was designed to understand the seasonal behavior of polar stratospheric ozone as it evolves from very high concentrations in spring to very low concentrations in autumn. During the campaign, the NASA ER-2 research aircraft was deployed from three locations: the NASA Ames Research Center, Moffett Field, California; Fort Wainwright U. S. Army Base, Fairbanks, Alaska; and Barbers Point Naval Air Station, Hawaii. During the 35 flights between March and September 1997, a suite of chemical species was measured from the ER-2 [*Newman et al.*, 1999]. In this study, we use the O_3, CO, and H_2O data from the 19 flights based at Fairbanks, Alaska (∼65°N, 147°W), which provided 38 ascending and descending profile measurements across the tropopause and covered the vertical range of 5 to 18 km. These flights were between April and September, with the exception of August.

[14] In situ O_3 data is from the NOAA ultraviolet absorption spectrometer instrument [*Proffitt and McLaughlin*, 1983]. The estimated accuracy is ∼3%. CO measurements are made from the Aircraft Laser Infrared Absorption Spectrometer (ALIAS) [*Webster et al.*, 1994; *Herman et al.*, 1999]. The measurement accuracy for CO is better than 10%. In situ water vapor data used in this analysis are from the Harvard Lyman-α hygrometer [*Weinstock et al.*, 1994]. The data have been shown to have an accuracy of ±5% [*Hintsa et al.*, 1999]. In this study, all data have been averaged over 10 s, leading to a horizontal resolution of ∼2 km and a vertical resolution of 0.1–0.2 km. The use of these data to characterize the chemical transition across the tropopause has been described in detail by *Pan et al.* [2004].

3. Model Diagnostics

[15] Results of four model runs are selected to compare with each other and with the ER-2 data. As described in section 2, they are MOZART-3 driven by ECMWF operational (Op) and reanalysis (EXP471) fields and WACCM3 in two different horizontal grid resolutions. To simplify the terminology, we designate the MOZART-3 with Op meteorological fields as case 1, MOZART-3 with EXP471 meteorological fields as case 2, WACCM3 using the 1.9 × 2.5 grid as case 3 and WACCM3 using the 4 × 5 grid as case 4. These four cases are summarized in Table 1. The model profiles are selected to be similar in location and sampling to the ER-2 data. Spatially, we selected profiles at 65°N latitude, within ±5° longitude range of 150°W, and up to the 70 hPa pressure level. We selected 3 days each month (5th, 15th, and 25th) for the five months coincident with the months of ER-2 flights. The number of data points from each case varies because of the difference in horizontal and vertical resolutions of the model runs. There are 75 profiles in cases 1–3 and 45 in case 4. Cases 1 and 2 have more data points than case 3 because of the higher vertical resolution.

3.1. Diagnostic 1: Profile Comparisons Using Relative Altitude Coordinates

[16] We use O_3, CO and H_2O to examine the chemical transition between the troposphere and stratosphere. All three trace gases exhibit rapid changes in their mixing ratios across the tropopause due to their respective chemical sources/sinks. Their lifetimes in this region are sufficiently

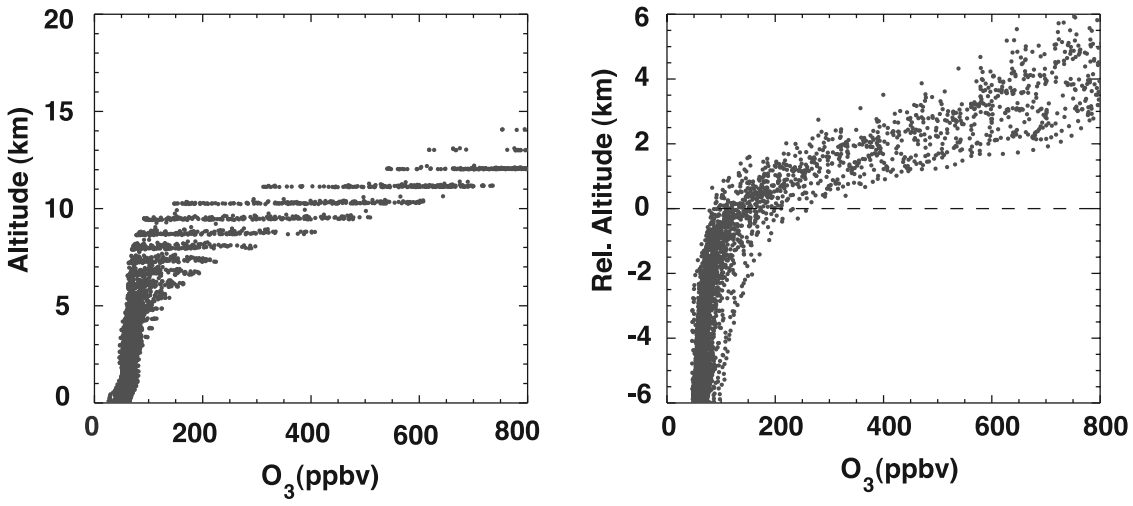

Figure 1. O_3 profiles near 65°N from the MOZART-3 model using ECMWF Op winds (left) in altitude coordinates and (right) in relative altitude (RALT) coordinates.

long to be affected by transport. In addition, H_2O is sensitive to the temperature in the tropopause region, providing additional diagnostic information for the models. Because the change in tracer profiles is strongly correlated with the tropopause level, it is useful to use a tropopause-referenced coordinate when examining the statistical behavior. On the basis of the vertical behavior of the data, we choose to use the altitude relative to the thermal tropopause level as the vertical coordinate, and refer to it as the relative altitude (RALT). This coordinate system has been used in a statistical representation of ozonesonde data [*Logan*, 1999], and the advantage of using this coordinate has been discussed further using aircraft in situ measurements [*Pan et al.*, 2004].

[17] As in the case of observational data analyses, RALT provides a better representation for model profiles, and this is demonstrated by an example in Figure 1. The ozone profiles from the case 1 model results are displayed in both altitude and RALT coordinate in Figure 1. The change of ozone across the tropopause coupled with the variability of tropopause height makes the profiles in regular altitude spread out in the UTLS region (~5–12 km). On the other hand, the change of ozone is much more compact in RALT coordinates. The use of RALT removes most of the day-by-day variability in the ozone profiles introduced by meteorological variability and facilitates comparisons between observations made under different meteorological conditions and with models.

[18] With the help of RALT, we compare the model profiles in the UTLS region with that observed by the ER-2. The ER-2 results are displayed in Figure 2. The model results from all four cases are given in Figure 3, with the mean and standard deviation from both model profiles and the ER-2 data superimposed. Figure 2 shows that the ER-2 profiles exhibit a sharp change across the tropopause in all three species. This sharp change is characterized by the ~100 ppbv mean value of ozone for the 1 km layer below the tropopause and ~300 ppbv for the 1 km layer above. Similarly, the CO profiles have a ~100 ppbv mean for the 1 km layer below the tropopause and ~40 ppbv for the 1 km layer above. H_2O profiles have a ~80 ppmv mean for the 1 km layer below the tropopause and ~20 ppmv mean for the layer above. Qualitatively, this transition is exhibited in the model profiles for all four cases (Figure 3) but it is less sharp. Quantitatively, differences exist between each model and the observations. In particular, the case 1 results produced much higher CO and H_2O values and lower ozone in the lower stratosphere. Cases 3 and 4, on the other hand, underestimate the tropospheric CO levels. In case 4, the transition from troposphere to stratosphere is less distinct in all three tracer profiles, with the region of 2 km below tropopause showing more stratospheric influence. These aspects will be discussed later in the paper.

3.2. Diagnostic 2: Tracer-Tracer Correlations

[19] Using largely aircraft in situ measurements, tracer-tracer correlation has been shown to be an effective tool for identifying the chemical transition between the stratosphere and troposphere, and the influence of mixing in the tropopause region [*Fischer et al.*, 2000; *Zahn et al.*, 2000; *Zahn and Brenninkmeijer*, 2003; *Hoor et al.*, 2002, 2004; *Pan et al.*, 2004; *Hegglin et al.*, 2006]. In this section, we explore the use of this tool to diagnose model performance. Two pairs of tracers, O_3-CO and O_3-H_2O, are used in this analysis.

[20] Figure 4 displays observed and modeled O_3-CO relationship. We first describe the characteristics of the observed correlations (upper left of Figure 4). The observed O_3-CO relationship is approximately "L" shaped, and consists of a stratospheric branch and a tropospheric branch, each with an approximate linear relationship between the two tracers. In the stratospheric branch, ozone spans a large dynamical range (~400–1200 ppbv) but CO exhibits small variability, while in the tropospheric branch the opposite is true. Between the two branches, there is a transition region marked by "mixing lines," a set of points of transitional chemical values between the stratospheric and the tropospheric populations, consistent with the influence of mixing between the stratosphere and troposphere. Furthermore, the color change in the transition region (based on the location of observation relative to the thermal tropopause, green for

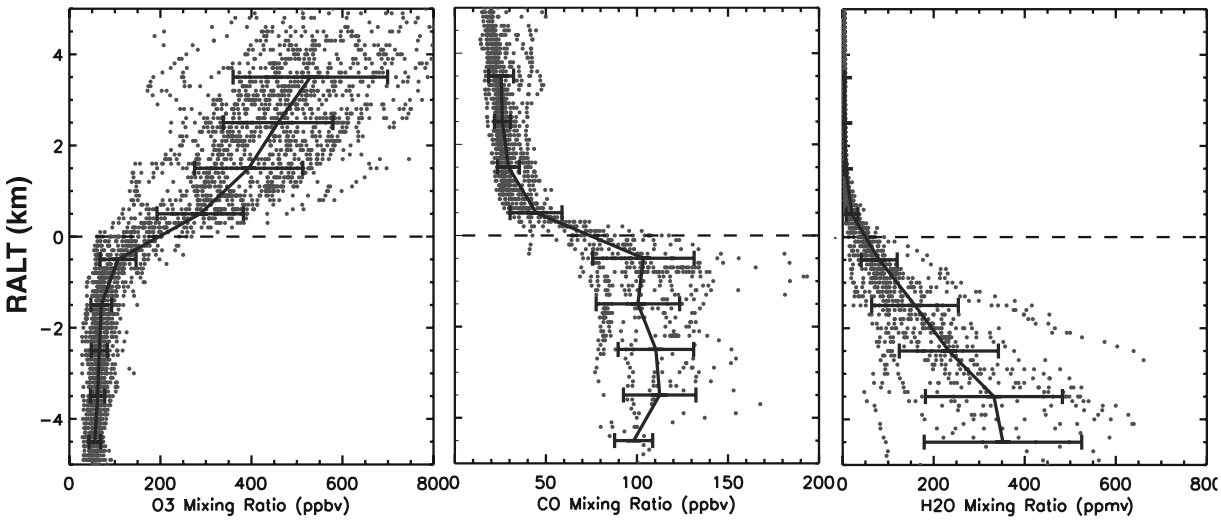

Figure 2. O_3, CO and H_2O profiles from ER-2 measurements near 65°N in RALT coordinates. The solid lines are the mean and standard deviation for each 1 km layer.

below and red for above) indicates that the thermal tropopause is located near the center of the mixing lines.

[21] To quantify these two empirically identified branches, we represent the branches by solid lines in the figures, derived from a fit to the data (linear for the tropospheric branch, and quadratic for the stratospheric branch). The fit for the stratospheric branch is produced using data with a selection criterion of CO < 25 ppbv. The fit for the tropospheric branch is produced using data selected by a criterion of O_3 < 70 ppbv. The range of 3σ of the fit is marked by the dotted lines. In addition, we marked the region of mixing by a straight line (light blue). The end points of this line are 400 ppbv of ozone on the stratospheric branch and 120 ppbv of CO on the tropospheric branch, respectively. These are the starting points where a significant fraction (10% or more) of the data is outside the 3σ range. We use this line as a proxy for the observed mixing lines. Together, the branches and the mixing line form a statistical reference for model evaluations. The parameters of the fits are given in Appendix A.

[22] Using this statistical reference, we now examine the characteristics of the model results from the model cases 1–3 (Figure 4). The result of case 4 is very similar to case 3 and is not shown. Qualitatively, all model cases approximately reproduce the "L" shaped tracer relationship. The common features are consistent with the observations, showing compact tracer relationships with the thermal tropopause located near the corner of the "L" (indicated by the position of the change from green to red in the tracer space (~200 ppbv ozone).

[23] Quantitatively, significant differences exist between models and observations. The stratospheric branch in case 1, in particular, shows a significant deviation from the observations. This is a different view of the same bias shown in the tracer profiles (Figure 3), and it is an indication of too much tropospheric influence in the lower stratosphere. This bias is significantly reduced in case 2, wherein the reanalysis data (EXP471) are used. A similar "excess transport" effect was found in a stratospheric study using these two meteorological data sets [*Monge-Sanz et al.*, 2007]. The excessive transport is likely a result of the assimilated wind field in the ECMWF Op meteorological data. We speculate that the data assimilation process generated a noisier wind field in the process of making adjustments with observations and maintaining balance using the dynamical equations. The noises produced artificial eddies and contributed to the excess transport across the tropopause. The excess transport is likely produced quasi-isentropically, as oppose to convectively, as suggested by the high CO and H_2O in the entire range of lower stratosphere shown in Figure 3 and the scatter in the stratospheric branch in Figures 4 and 5. Similar symptoms of excess transport were discussed by *Schoeberl et al.* [2003] in a study of stratospheric transport, where they showed that a CTM driven by assimilated meteorological field will not produce a realistic trace gas distribution and that the age spectrum is too broad. A more detailed analysis of wave activity is desirable to provide definitive explanations and to characterize the limitations of the wind fields from operational analyses.

[24] Case 3 produces compact stratospheric and tropospheric branches that are in good agreement with the observations. The tropospheric branch, in this case, however, shows a smaller range of CO variability (as well as a low bias, as shown in Figure 3) than observed. This is due to the omission of NMHC, which are significant sources for tropospheric CO, in the chemistry mechanism used in the WACCM3 runs. As a consequence, the slope of the mixing lines in case 3 is significantly different from the observations. There is a question whether the good agreement of the stratospheric branch in case 3 is a result of low tropospheric CO. The profiles in RALT shown in Figure 3 argues against this, because the ozone profile in the lower stratosphere for this case agrees well with the observations and does not indicate too much tropospheric influence. This issue will be further examined in future WACCM3 runs.

[25] The correlation of the second tracer pair, O_3-H_2O (Figure 5) also form an "L" shaped relationship in the UTLS region. Similar to the O_3-CO correlation, there is a qualitative agreement between the models (cases 1–3) and

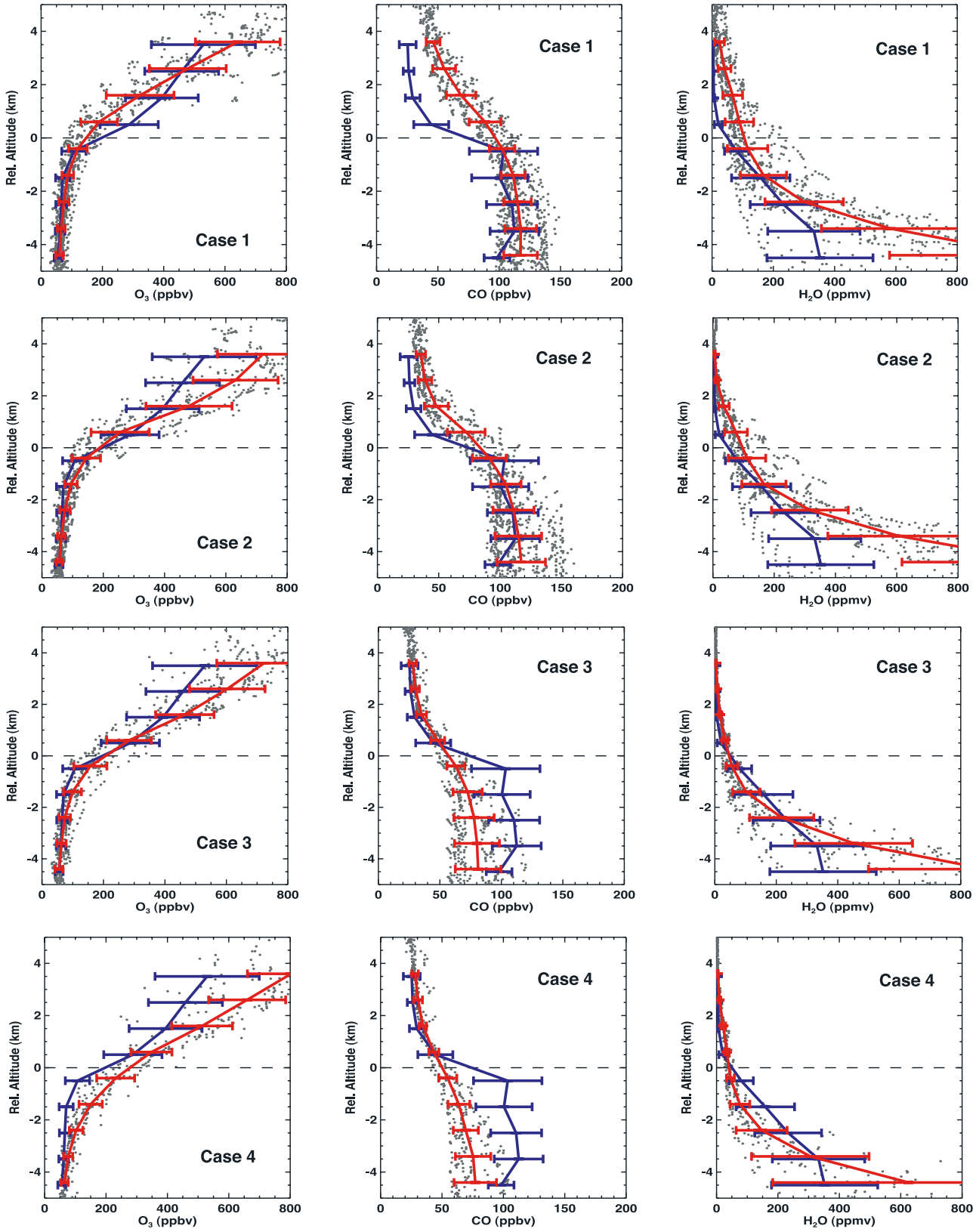

Figure 3. O_3, CO and H_2O profiles from all four cases of model runs in RALT coordinates (gray points). The blue lines are the mean and standard deviations of the ER-2 profiles, and the red lines are the mean and standard deviations of the model results.

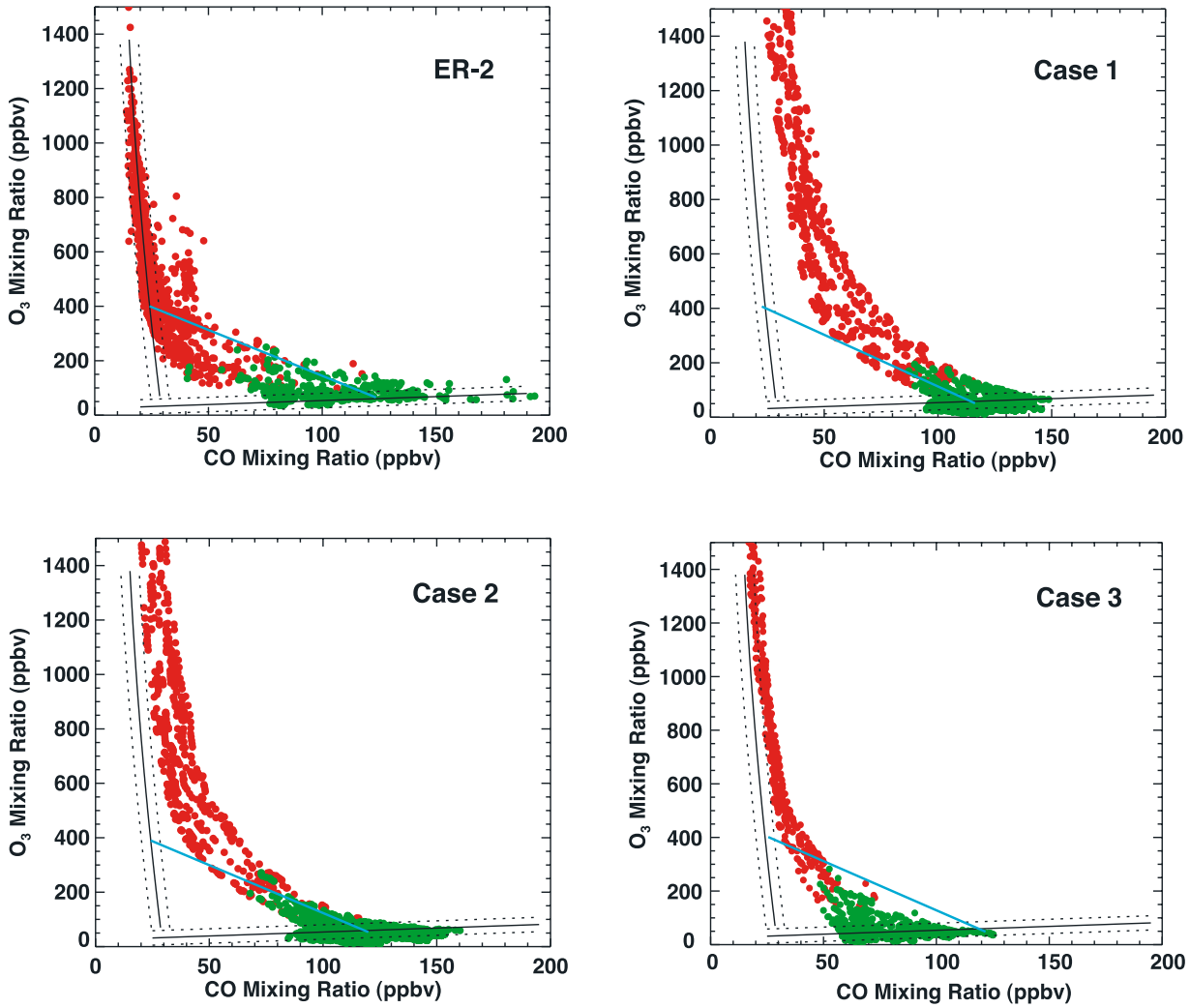

Figure 4. Comparisons of O_3-CO relationship between ER-2 observations and the results of 3 model runs. In all cases, red (green) points are above (below) the thermal tropopause, the solid and dotted lines are fit to the ER-2 stratospheric and tropospheric points, respectively, and the range of 3 sigma standard deviations. The selection criteria for the points in the fit are explained in the text. The light blue line for the ER-2 plot is drawn to mark the border of the mixing region in the tracer space. The end points of the line are 400 ppbv of ozone on the stratospheric branch and 120 ppbv of CO on the tropospheric branch, respectively. These are the location in the tracer space where a significant number of data points (>10%) deviates from the compact relationship (3σ from the fit).

the observations. In this case, the temperature of the tropopause region also plays a significant controlling role. Using a similar criterion as in Figure 4, we identify the end points of the proxy mixing line to be 400 ppbv of ozone and 100 ppmv of H_2O. The observations in the tracer-tracer space show no significant fraction of data outside the region of two branches and the mixing region at the corner of the "L." In contrast, the model cases all show a significant fraction of the data points outside the region defined by the observations. The case 1 results in particular show significant scatter away from the compact relationship marked by unreasonably high values of H_2O in the region of high O_3. Qualitatively, cases 2 and 3 produce much better agreement with the observations. However, in both cases, the mixing lines occupy a much larger range in tracer space than observed. For example, the upper end point of the observed mixing line is ~400 ppbv of ozone in the observations but ~700 ppbv or greater in the models. This is an indication that the transition regions in these models are poorly resolved. This is discussed in more detail in next section.

[26] Note that the slopes of the mixing lines are expected to vary with season, because their end points depend on the source strength of the tracers involved. Seasonal changes of the UTLS transport will also impact the shape of the mixing lines, as discussed by *Hoor et al.* [2002, 2004]. In the case of the O_3-H_2O correlation presented in Figure 5, we expect a seasonal variation of the lower end point due to the sensitivity of H_2O to the temperature of the tropopause region. This is indeed found to be the case when the O_3-H_2O relationship observed by the ER-2 is examined for each month available from the POLARIS Campaign (April–September). There is a significant change in the

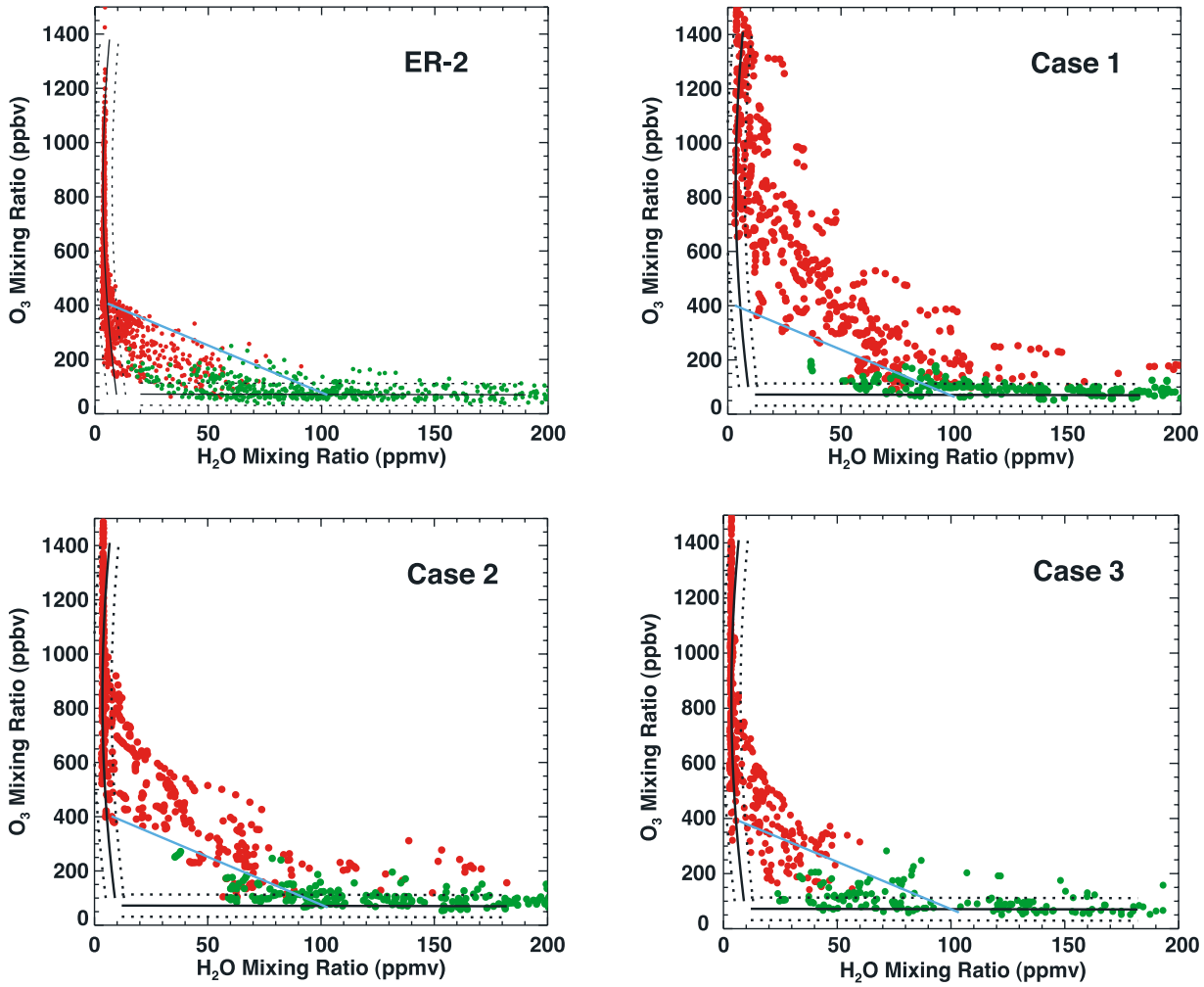

Figure 5. Same as Figure 4 but for O_3-H_2O relationship. The end points of the mixing border line (light blue) are 400 ppbv of ozone and 100 ppmv of water vapor.

lower end point of the mixing line, with a minimum ~50 ppmv of H_2O in April, and a maximum ~100 ppmv in July. The upper end point of this relationship also showed variation, with a maximum in April ~450 ppbv of O_3, and a minimum in September ~350 ppbv of O_3. This behavior is consistent with the seasonal cycle of ozone in the lowermost stratosphere. These changes are not consistently resolved by the models, since the overall discrepancies between the models and the observations, as shown in Figures 4 and 5, are much larger then the magnitude of the observed seasonal variations. As the models improve, the seasonal variation of the mixing lines should be used as an additional diagnostic for model performance.

3.3. Diagnostic 3: Sharpness of the Transition

[27] We further analyze the spatial extent of the transition region represented in the models using the method presented by *Pan et al.* [2004]. The transition region from the O_3-CO relationship based on ER-2 data shows a fairly compact spatial extent once the RALT coordinates are used and extends approximately ±1 km around the thermal tropopause. In Figure 6, we show a similar analysis using the O_3-H_2O relationship and comparing ER-2 observations during POLARIS with model results from cases 3 and 4. Data points used in Figure 6 are the same as those in Figure 5. The difference is that we are now looking beyond the identification of the stratospheric and tropospheric branches, represented by the green and red points in Figure 5. The focus now is to identify the distribution of the transitional points, represented by the blue points in Figure 6. These transitional points are selected using the criterion of being more than 3σ (dotted lines) away from the fit lines defining both the stratosphere and tropospheric branches (solid lines). The case 1 result is not shown, because the compact stratospheric branch is not well reproduced in the model for that case, as indicated in Figure 5 (upper right). Case 2 is not shown either because the overall characteristics in that case are very similar to case 4.

[28] The histograms in Figure 6 show that, consistent with the ER-2 observations, the distribution of the transitional points from models is centered near the thermal tropopause. This is a significant result, since no specific tropopause information was incorporated in the chemistry modules, validating the correct representation of the chemistry and the change in transport characteristics across the

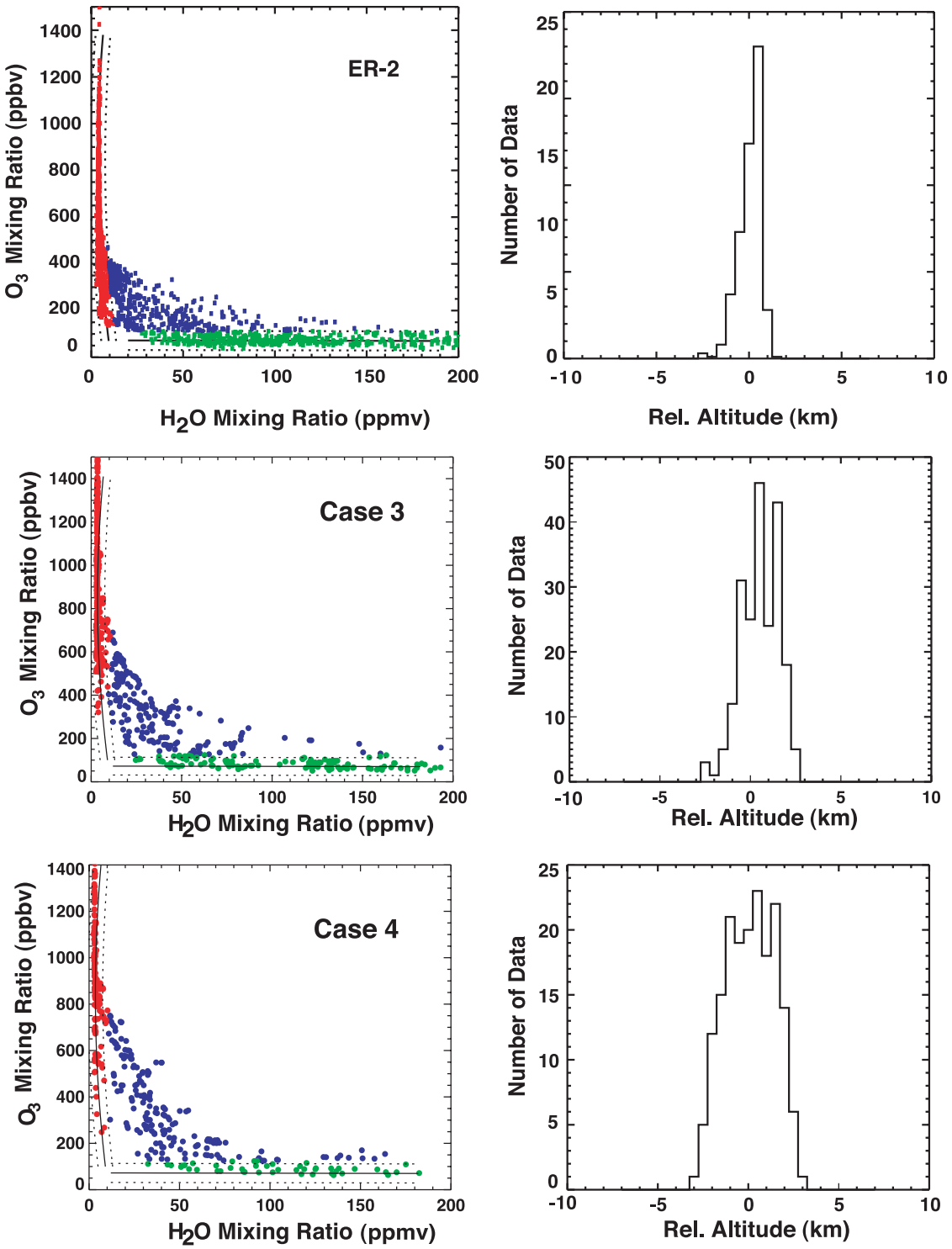

Figure 6. Sharpness of the chemical transition from ER-2 observations and WACCM3 model results. (left) Red and green points are identified as stratospheric and tropospheric, respectively (within 3σ from the fit). The blue points are identified as transitional points, produced primarily by mixing of stratospheric and tropospheric air. (right) Histograms show the distributions of the blue points in RALT space, providing a quantitative measure of the sharpness of the chemical transition across the tropopause.

tropopause in the models. The modeled transition layer, however, is much broader, reflecting a limitation of the model in resolving the rapid change in tracer field across the tropopause. This is consistent with the significant difference between models and observations in the locations of the mixing lines in the tracer space.

[29] Among the factors that contribute to the broader transition layer by the models, the most obvious one is

Table A1. Mean O_3 and CO Profiles and Standard Deviations in RALT Coordinate

	O_3		CO		H_2O	
RALT	Mean	σ	Mean	σ	Mean	σ
−4.5	55.8	12.9	98.2	10.5	352.1	173.1
−3.5	62.0	15.8	112.5	19.9	332.3	150.4
−2.5	65.7	17.7	110.4	20.7	233.3	108.9
−1.5	70.1	22.8	100.5	22.9	158.9	95.2
−0.5	107.0	39.6	103.5	27.9	80.2	39.5
0.5	287.4	94.9	44.6	14.3	20.5	12.8
1.5	393.9	118.8	29.5	6.0	6.2	2.2
2.5	458.6	120.5	26.1	4.4	4.4	0.7
3.5	529.5	169.8	25.4	6.8	4.2	0.6

the limitation from the vertical resolution used to represent the tropopause region. In general, we expect the agreement between the model and observations to improve with increased vertical resolution in this region, but other factors, such as the wind field, can also be important, as discussed the section 3.2.

[30] The difference between cases 3 and 4 in their representations of the transition layer also highlights the importance of horizontal resolution. These two runs used different horizontal grids but otherwise are identical. Case 3 produces a transition layer approximately ±1.5 km around the tropopause while case 4 has a much broader transition layer, broader than ±2 km (Figure 6). This suggests that the transition layer is not solely produced by vertical mixing. Horizontal mixing plays a significant role in the formation of the transition layer, and the horizontal grid resolution will impact the vertical behavior. A similar observation was made in a mechanistic model study by *Polvani et al.* [2004], where it was demonstrated, within the context of idealized synoptic lifecycles, that horizontal resolution and horizontal diffusion can have dramatic effects on the amplitude of the vertical velocities in a model.

4. Conclusions and Discussions

[31] We have described three diagnostics for evaluating the representation of the chemical transition and distributions in the extratropical UTLS by CTMs and CCMs using NCAR's MOZART-3 and WACCM3 as examples. We have demonstrated the use of RALT and tracer-tracer correlations to facilitate comparisons of models and data. They both serve to create a space where the impact of meteorological variability in the region is minimized and the climatological features of the chemical distribution are highlighted. We further demonstrated an approach to quantifying the sharpness of the chemical transition across the tropopause using tracer relationships. These analyses are performed empirically, as a first step, for the latitude of 65°N only. As more measurements become available, a global analysis would be possible and the use of source/sink/lifetime information will further produce a theoretical basis for the observed compact relationship.

[32] Both the profile comparisons using RALT and the tracer correlation comparisons show that the chemical transition across the tropopause is qualitatively well represented in the selected NCAR models, MOZART-3 and WACCM3. The transition is occurring near the thermal tropopause, shown both in profiles and tracer correlations, consistent with that concluded from the ER-2 measurements.

[33] Quantitatively, the modeled trace gas profiles and tracer relationships show significant differences, compared to the observations and among each other. These differences indicate that the meteorological field is a significant factor in determining how well the chemical distribution is reproduced in the UTLS region. Among the four cases we examined, the fully interactive CCM WACCM3 does a better job of modeling the tracer relationships in the lowermost stratosphere than the MOZART-3 runs driven by the ECMWF winds. The main difference between them is how the dynamics and chemistry are coupled; that is, one is an off-line model run driven by assimilated winds and the other a fully interactive model that uses winds derived by dynamical equations. The importance of the wind fields is further highlighted in the comparisons between cases 1 and 2, where the model runs used two different meteorological analyses and other wise identical. In particular, the chemical distribution in case 1 (MOZART-3 driven by ECMWF Op wind) shows too much tropospheric influence in the lowermost stratosphere. Results of using the ECMWF EXP471 reanalysis winds (case 2) show significant improvement in the agreement with observations. The main difference between these two analyses, as mentioned in section 2.1, is the enhanced background constraint to balance the wind field in EXP471. We speculate that this reduced the noise produced by the data assimilation in the operational analyses. These results are consistent with the age of air analysis by Kinnison et al. (submitted manuscript, 2006), where the age of air in the middleworld is too young when ECMWF Op field is used to drive MOZART-3.

[34] In addition, the chemical transitions at the tropopause in models are not as abrupt as in observations, indicating the need for further improvement of model vertical resolution near this transport boundary. Furthermore, the results of two WACCM3 runs that used the same vertical levels but a different horizontal grid ($1.9° \times 2.5°$ versus $4° \times 5°$) showed significant differences in their representation of the transition region. Although both reproduced the characteristics of the chemical transition across the tropopause, the transition is significantly broader in the case of coarser horizontal resolution. This result suggests that the horizontal resolution of the model is also an important factor in the accurate representation of chemical distributions near the tropopause.

[35] Comparison of case 2 and case 3 also shows the importance of chemistry for the UTLS region. While the upper tropospheric CO is too low in case 3, because of the omission of NMHC chemistry, the observed tropospheric branch in the O_3-CO relationship is well reproduced in case 2.

[36] In addition to the wind field and model resolution, other factors, such as the method of calculating advection, could contribute to the diffusiveness across the tropopause.

Table A2. Parameters for Identifying the Stratospheric Branch of Tracer-Tracer Correlations[a]

x	a_0	a_1	a_2	σ_x
CO	29.58	−0.015	3.20×10^{-6}	1.35
H_2O	10.58	−0.014	9.95×10^{-6}	1.34

[a]The coefficients given in this table are defined as $x = a_0 + a_1 y + a_2 y^2$, where y is O_3, and x is CO or H_2O. The standard deviation, σ_x, is also given in the table, which was used to define the width of the stratospheric branch and to select the transitional points in the diagnostic 3.

Table A3. Parameters for Identifying the Tropospheric Branch of Tracer-Tracer Correlations[a]

x	b_0	b_1	σ_y
CO	24.54	0.29	8.86
H_2O	72.54	−0.014	13.68

[a]The coefficients are defined as $y = b_0 + b_1 x$. Same as in the previous table, y is O_3, and x is CO or H_2O. The standard deviation, σ_y, is used to define the width of the tropospheric branch.

Future model runs with improved resolution and wind fields will allow us to examine the role of these additional parameters in simulating observed chemical transition across the tropopause.

[37] Note that the diagnostics presented here are derived from very limited data. To expand this type of analyses to a broader latitude range and to cover all seasons, more aircraft measurements with adequate vertical coverage in the UTLS are essential. It is also important to explore the use of new generation satellite data, such as those provided by the Atmospheric Infrared Sounder (AIRS), the Microwave Limb Sounder (MLS) and Tropospheric Emission Spectrometer (TES) on the NASA EOS satellites. Once the resolution and accuracy of these data are characterized, they have the potential to provide information for model validation on a global scale.

Appendix A: ER-2 Data Derived Parameters for Model Diagnoses

[38] In this appendix, we provide the measurements derived parameters used in the three diagnostics described in the paper. Table A1 gives the parameters used to produce the mean profile and standard deviation in Figure 3. Table A2 gives the parameters used to define the stratospheric branch, and Table A3 gives the parameters used to define the tropospheric branches in the tracer-tracer correlations in Figures 4–6.

[39] **Acknowledgments.** This work is supported in part by the National Science Foundation through its support to the University Corporation for Atmospheric Research (UCAR). The authors thank W. J. Randel and B. A. Ridley for helpful comments and suggestions. In addition, the authors thank Beatriz Monge-Sanz and Adrian Simmons for providing ECMWF EXP471 assimilation data. We would also like to thank Ulrike Niemeier and Thomas Diehl for providing additional ECMWF assimilation data.

References

Austin, J., et al. (2003), Uncertainties and assessments of chemistry-climate models of the stratosphere, *Atmos. Chem. Phys.*, *3*, 1–27.

Brasseur, G. P., D. A. Hauglustaine, S. Walters, P. J. Rasch, J.-F. Muller, C. Granier, and X. X. Tie (1998), MOZART: A global chemical transport model for ozone and related chemical tracers: 1. Model description, *J. Geophys. Res.*, *103*, 28,265–28,289.

Collins, W. D., et al. (2004), Description of the NCAR Community Atmosphere Model (CAM3), Natl. Cent. for Atmos. Res., Boulder, Colo.

Emmons, L., et al. (2003), The budget of tropospheric ozone during TOPSE from two chemical transport models, *J. Geophys. Res.*, *108*(D8), 8372, doi:10.1029/2002JD002665.

Eyring, V., et al. (2005), A strategy for process-oriented validation of coupled chemistry-climate models, *Bull. Am. Meteorol. Soc.*, *86*, 1117–1133.

Fischer, H., F. G. Wienhold, P. Hoor, O. Bujok, C. Schiller, P. Siegmund, M. Ambaum, H. A. Scheeren, and J. Lelieveld (2000), Tracer correlations in the northern high latitude lowermost stratosphere: Influence of cross-tropopause mass exchange, *Geophys. Res. Lett.*, *27*, 97–100.

Forkman, P., P. Ericksson, A. Winnberg, R. R. Garcia, and D. E. Kinnison (2003), Longest continuous ground-based measurements of mesospheric CO, *Geophys. Res. Lett.*, *30*(10), 1532, doi:10.1029/2003GL016931.

Garcia, R. R., D. Marsh, D. Kinnison, B. Boville, and F. Sassi (2007), Simulation of secular trends in the middle atmosphere, 1950–2003, *J. Geophys. Res.*, doi:10.1029/2006JD007485, in press.

Gettelman, A., D. E. Kinnison, G. Brasseur, and T. Dunkerton (2004), Impact of monsoon circulations on the upper troposphere and lower stratosphere, *J. Geophys. Res.*, *109*, D22101, doi:10.1029/2004JD004878.

Hauglustaine, D. A., G. P. Brasseur, S. Walters, P. J. Rasch, J.-F. Muller, L. K. Emmons, and M. A. Carroll (1998), MOZART: A global chemical transport model for ozone and related chemical tracers: 2. Model results and evaluation, *J. Geophys. Res.*, *103*, 28,291–28,335.

Haynes, P., J. Scinocca, and M. Greenslade (2001), Formation and maintenance of the extratropical tropopause by baroclinic eddies, *Geophys. Res. Lett.*, *28*(22), 4179–4182.

Hegglin, M. I., D. Brunner, T. Peter, P. Hoor, H. Fischer, J. Staehelin, M. Krebsbach, C. Schiller, U. Parchatka, and U. Weers (2006), Measurements of NO, NO_y, N_2O, and O_3 during SPURT: Seasonal distributions and correlations in the lowermost stratosphere, *Atmos. Chem. Phys.*, *6*, 1331–1350.

Herman, R. L., et al. (1999), Measurements of CO in the upper troposphere and lower stratosphere, *Chemosphere Global Change Sci.*, *1*, 173–183.

Hintsa, E. J., et al. (1998), Troposphere-to-stratosphere transport in the lowermost stratosphere from measurements of H_2O, CO_2, N_2O and O_3, *Geophys. Res. Lett.*, *25*(14), 2655–2658.

Hintsa, E. J., E. M. Weinstock, J. G. Anderson, R. D. May, and D. F. Hurst (1999), On the accuracy of in situ water vapor measurements in the troposphere and lower stratosphere with the Harvard Lyman-α hygrometer, *J. Geophys. Res.*, *104*, 8183–8189.

Holton, J. R., P. H. Haynes, M. E. McIntyre, A. R. Douglass, R. B. Rood, and L. Pfister (1995), Stratosphere-troposphere exchange, *Rev. Geophys.*, *33*, 403–439.

Hoor, P., H. Fischer, L. Lange, J. Lelieveld, and D. Brunner (2002), Seasonal variations of a mixing layer in the lowermost stratosphere as identified by the CO-O_3 correlation from in situ measurements, *J. Geophys. Res.*, *107*(D5), 4044, doi:10.1029/2000JD000289.

Hoor, P., C. Gurk, D. Brunner, M. I. Hegglin, H. Wernli, and H. Fischer (2004), Seasonality and extent of extratropcial TST derived from in-situ CO measurements during SPURT, *Atmos. Chem. Phys.*, *4*, 1427–1442.

Horowitz, L., et al. (2003), A global simulation of tropospheric ozone and related tracers: Description and evaluation of MOZART, version 2, *J. Geophys. Res.*, *108*(D24), 4784, doi:10.1029/2002JD002853.

Hsu, J., M. J. Prather, O. Wild, J. K. Sundet, I. S. A. Isaksen, E. V. Browell, M. A. Avery, and G. W. Sachse (2004), Are the TRACE-P measurements representative of the western Pacific during March 2001?, *J. Geophys. Res.*, *109*, D02314, doi:10.1029/2003JD004002.

Kulawik, S. S., et al. (2006), TES atmospheric profile retrieval characterization: An orbit of simulated observations, *IEEE Trans. Geosci. Remote Sens.*, *44*(5), 1324–1333.

Lin, S.-J. (2004), A "vertically lagrangian" finite-volume dynamical core for global atmospheric models, *Mon. Weather Rev.*, *132*, 2207–2293.

Lin, S.-J., and R. B. Rood (1997), An explicit flux-form semi-Lagrangian shallow-water model on the sphere, *Q. J. R. Meteorol. Soc.*, *123*, 2477–2498.

Logan, J. (1999), An analysis of ozonesonde data for the troposphere: Recommendations for testing 3-D models and development of a gridded climatology for tropospheric ozone, *J. Geophys. Res.*, *104*(D13), 16,115–16,150.

Marcy, T., et al. (2004), Quantifying stratospheric ozone in the upper troposphere with in situ measurements of HCl, *Science*, *304*, 261–265.

Monge-Sanz, B. M., M. P. Chipperfield, A. J. Simmons, and S. M. Uppala (2007), Mean age of air and transport in a CTM: Comparison of different ECMWF analyses, *Geophys. Res. Lett.*, *34*, L04801, doi:10.1029/2006GL028515.

Newman, P. A., D. W. Fahey, W. H. Brune, and M. J. Kurylo (1999), Preface to special section: Photochemistry of Ozone Loss in the Arctic Region in Summer (POLARIS), *J. Geophys. Res.*, *104*(D21), 26,481–26,495.

Pan, L. L., W. J. Randel, B. L. Gary, M. J. Mahoney, and E. J. Hintsa (2004), Definitions and sharpness of the extratropical tropopause: A trace gas perspective, *J. Geophys. Res.*, *109*, D23103, doi:10.1029/2004JD004982.

Pan, L. L., P. Konopka, and E. V. Browell (2006), Observations and model simulations of mixing near the extratropical tropopause, *J. Geophys. Res.*, *111*, D05106, doi:10.1029/2005JD006480.

Park, M., W. R. Randel, D. E. Kinnison, R. R. Garcia, and W. Choi (2004), Seasonal variations of methane, water vapor, ozone, and nitrogen dioxide near the tropopause: Satellite observations and model simulations, *J. Geophys. Res.*, *109*, D03302, doi:10.1029/2003JD003706.

Polvani, L. M., R. K. Scott, and S. J. Thomas (2004), Numerically converged solutions of the global primitive equations for testing the dynamical core of atmospheric GCMs*, *Mon. Weather Rev.*, *11*, 2539–2552.

Proffitt, M. H., and R. J. McLaughlin (1983), Fast-response dualbeam UV-absorption ozone photometer suitable for use on stratospheric balloons, *Rev. Sci. Instrum.*, *54*, 1719–1728.

Rasch, P. J., N. M. Mahowald, and B. E. Eaton (1997), Representations of transport, convection, and the hydrological cycle in chemical transport models: Implications for the modeling of short-lived and soluble species, *J. Geophys. Res.*, *102*, 28,127–28,138.

Ridley, B. A., et al. (2004), Convective transport of reactive constituents to the tropical and mid-latitude tropopause region: I. Observations, *Atmos. Environ.*, *38*, 1259–1274.

Sanders, S. P., et al. (2003), Chemical kinetics and photochemical data for use in atmospheric studies, *JPL Publ. 02-25*, NASA Jet Propul. Lab., Pasadena, Calif.

Sassi, F., D. Kinnison, B. A. Boville, R. R. Garcia, and R. Roble (2004), The effects of El Niño–Southern Oscillation on the dynamical, thermal and chemical structure of the middle atmosphere, *J. Geophys. Res.*, *109*, D17108, doi:10.1029/2003JD004434.

Schoeberl, M. R., A. R. Douglass, Z. Zhu, and S. Pawson (2003), A comparison of the lower stratospheric age spectra derived from a general circulation model and two data assimilation systems, *J. Geophys. Res.*, *108*(D3), 4113, doi:10.1029/2002JD002652.

Webster, C. R., R. D. May, C. A. Trimble, R. G. Chave, and J. Kendall (1994), Aircraft (ER-2) laser infrared absorption spectrometer (ALIAS) for in situ stratospheric measurements of HCl, N_2O, CH_4, NO_2, and HNO_3, *Appl. Opt.*, *33*, 454–472.

Weinstock, E. M., et al. (1994), New fast response photofragment fluorescence hygromenter for use on the NASA ER-2 and the Perseus remotelypiloted aircraft, *Rev. Sci. Instrum.*, *65*, 3544–3554.

Zahn, A., and C. A. M. Brenninkmeijer (2003), New directions: A chemical tropopause defined, *Atmos. Environ.*, *37*, 439–440.

Zahn, A., et al. (2000), Identification of extratropical two-way troposphere-stratosphere mixing based on CARIBIC measurements of O_3, CO, and ultrafine particles, *J. Geophys. Res.*, *105*, 1527–1535.

G. P. Brasseur, R. R. Garcia, D. E. Kinnison, and L. L. Pan, Atmospheric Chemistry Division, National Center for Atmospheric Research, Boulder, CO 80305, USA. (liwen@ucar.edu)

J. C. Wei, QSS Group, Inc., Lanham, MD 20706, USA.

D. J. Wuebbles, Department of Atmospheric Sciences, University of Illinois at Urbana-Champaign, 105 S. Gregory, Urbana, IL 61801, USA.